HHS Public Access

Author manuscript

Nat Neurosci. Author manuscript; available in PMC 2010 March 03.

Published in final edited form as:

Nat Neurosci. 2009 August ; 12(8): 973–980. doi:10.1038/nn.2375.

Genesis of cerebellar interneurons and the prevention of neural DNA damage require XRCC1

Youngsoo Lee, **Sachin Katyal**, **Yang Li**, **Sherif F. El-Khamisy**[1], **Helen R. Russell**, **Keith W. Caldecott**[1], and **Peter J. McKinnon**[*]

Department of Genetics and Tumor Cell Biology, St Jude Children's Research Hospital, Memphis TN 38105, USA

[1] Genome Damage and Stability Unit, University of Sussex, Brighton, UK

Abstract

Defective responses to DNA single strand breaks underpin various neurodegenerative diseases. However, the exact role of this repair pathway during development and maintenance of the nervous system is unclear. Using murine neural-specific inactivation of Xrcc1, a factor critical for the repair of DNA single strand breaks, we identified a profound neuropathology characterized by the loss of cerebellar interneurons. This cell loss was linked to p53-dependent cell cycle arrest and occurred as interneuron progenitors commenced differentiation. Loss of Xrcc1 also led to the persistence of DNA strand breaks throughout the nervous system and abnormal hippocampal function. Collectively, these data detail the first *in vivo* link between DNA single strand break repair and neurogenesis, and highlight the diverse consequences of specific types of genotoxic stress in the nervous system.

Keywords

Xrcc1; cerebellum; interneurons; DNA repair; DNA strand breaks

Introduction

The ability to respond to genotoxic stress is necessary for development of the nervous system. Defective responses to DNA damage can result in a multitude of human syndromes that feature pronounced neuropathology1-3. For example, spinocerebellar ataxia with axonal neuropathy (SCAN1) and ataxia with oculomotor apraxia (AOA1) are syndromes associated with single strand break repair (SSBR) defects and feature ataxia linked to cerebellar degeneration and neuropathy4-7. SCAN1 results from disruption of tyrosyl-DNA

[*] Correspondence should be addressed to Phone (901) 595-2700, Fax (901) 595-6035, peter.mckinnon@stjude.org.

Author Contributions Y.Lee and S.K. performed all experiments characterizing the Xrcc1-deficient mouse and contributed to writing the manuscript. Y.Li. and H.R.H. generated the mouse model and were responsible for colony production and maintenance with assistance from S.K and Y.Lee. S.F.E.-K and K.W.C. designed and performed experiments and contributed to preparation of the manuscript. P.J.M. was project leader and produced the final version of the manuscript.

Supplemental Data. Supplemental experimental procedures, twelve figures, one table and a Quicktime movie are associated with this article.

phosphodiesterase 1 (TDP1), an enzyme required for the 3′-end processing of certain DNA lesions5. In AOA1, mutations in Aprataxin (APTX) causes defects in the removal of 5′-adenylate-DNA intermediates that can occur during DNA ligation reactions3, 4. While these observations reveal the importance of addressing SSBs to avoid neuropathology, the general requirements for SSBR during neurogenesis is unknown.

XRCC1 is central to SSBR and interacts with multiple DNA repair factors including APTX and DNA polymerase β to process a DNA break for ligation involving DNA ligase III (Lig3)2. Because Xrcc1 null mice die around embryonic day 7 (E7)8, the physiological role of this repair factor remains unclear. To address this, we generated a conditional *Xrcc1* allele to assess the role of SSBR in the mouse nervous system. Here we demonstrate that *Xrcc1* is required for neurogenesis of cerebellar interneurons and for hippocampal homeostasis. We also found that *Xrcc1* deficiency lead to the progressive and persistent accumulation of strand breaks in mature neuronal populations. These data are fundamentally important for understanding the etiology and neuropathology associated with neurodegenerative diseases arising from defective DNA damage responses.

RESULTS

Conditional inactivation of *Xrcc1* in the nervous system

Germline deletion of *Xrcc1* results in early embryonic lethality precluding the analysis of Xrcc1 during development8. To circumvent this we used a cre/LoxP approach to generate a conditional *Xrcc1* allele (Fig. 1a,b and Suppl. Fig. 1). We initially examined the effect of *Xrcc1* inactivation throughout the embryo by intercrossing mice containing an $Xrcc1^{LoxP}$ allele with *Meox2-cre*, a line that expresses the cre recombinase in the epiblast layer9. This allowed us to determine if early lethality after germ-line deletion involved the placenta. $Xrcc1^{LoxP/LoxP}$*;Meox2-cre* embryos were malformed by E10 and displayed a high index of apoptosis throughout the embryo (Suppl. Fig. 1). We did not observe live $Xrcc1^{LoxP/LoxP}$*;Meox2-cre* embryos after E12.5, consistent with an essential embryonic function for Xrcc18.

To explore the link between defective SSBR repair and neurodegeneration2, 3, 10, we used *Nestin-cre*11, 12 to inactivate *Xrcc1* in the nervous system. Efficient deletion of *Xrcc1* in neural tissues in $Xrcc1^{LoxP/LoxP}$*;Nestin-cre* mice (hereafter referred to as $Xrcc1^{Nes\text{-}cre}$) was confirmed at the DNA, RNA and protein level (Fig. 1c,d and Suppl. Fig. 1). Repair of DNA strand breaks via Xrcc1-dependent SSBR and base excision repair (BER) is associated with Lig3 activity to reseal the DNA nick. Previous studies have reported that Lig3 levels are linked to Xrcc113. To determine if this occurs *in vivo* we performed Western analysis using anti-Lig3 antibody. Compared with control tissue extracts, $Xrcc1^{Nes\text{-}cre}$ cortex and cerebellum had drastically reduced Lig3 levels (Fig. 1d) indicating that loss of Xrcc1 results in reduced Lig3 levels.

Aside from a growth delay, $Xrcc1^{Nes\text{-}cre}$ mice did not show any other discernable defects such as cancer and the cause of premature death remains uncertain. However, adult $Xrcc1^{Nes\text{-}cre}$ mice developed pronounced neurological dysfunction characterized by progressive ataxia accompanied with episodic spasms (Suppl. Movie). $Xrcc1^{Nes\text{-}cre}$ animals

were born alive but showed slowed growth, smaller brain size and developed to only 75% in size and body weight to matched control animals (Fig. 1f). Magnetic resonance imaging analysis of *Xrcc1*$^{Nes\text{-}cre}$ mice revealed a pronounced reduction in cerebellar size compared to the rest of the brain, although the overall brain to body weight ratio was similar (Fig. 1g). *Xrcc1*$^{Nes\text{-}cre}$ animals generally survived up to four months of age (Fig. 1e).

Xrcc1 loss results in DNA repair deficiency in the brain

To assess the role of Xrcc1 in repairing DNA damage in the nervous system, we subjected neurons isolated from postnatal day 15 (P15) cerebella (Fig. 2a) to DNA repair assays using alkaline comet analysis (ACA). We found a four-fold increase in global DNA strand breaks in *Xrcc1*$^{Nes\text{-}cre}$ neurons over controls (Fig. 2b). To further characterize neuronal repair, we analyzed the effects of cultured post-mitotic cerebellar granule cell neurons (Fig. 2c,d and Suppl. Fig. 2a) and quiescent cortical astrocytes (Suppl. Fig. 2b) after exposure to exogenous genotoxic agents. Both *Xrcc1*-deficient neural cell types showed that a substantial proportion of DNA strand breaks induced by ionizing radiation (IR) or hydrogen peroxide (H_2O_2) remain unrepaired after prolonged recovery in genotoxic free conditions, or after methyl methanesulfonate (MMS) exposure, whereas repair was robust in control cells (Fig. 2c and Suppl. Fig. 2). Knockdown of XRCC1 also sensitizes human neurons to oxidative stress after menadione treatment14. Because Xrcc1 is critical for SSBR and IR and H_2O_2 produce 20-2,000 fold more SSBs than DSBs, our data indicate that *Xrcc1* loss in neural tissue result in a pronounced SSBR deficiency.

To further determine the consequence of Xrcc1 loss, we analyzed *Xrcc1*$^{Nes\text{-}cre}$ brains for the accumulation of DNA strand breaks. We used γH2AX as a marker for DNA damage; γH2AX is the phosphorylated version of histone H2AX which forms at DNA breaks to enhance DNA repair efficiency15. Although γH2AX typically marks DNA double strand breaks (DSBs)16, defective SSBR from Xrcc1 loss can result in DSBs that arise from the replication fork or transcriptional machinery colliding with SSBs, or random damage accumulation leading to adjacent breaks. During early neural development γH2AX occurred in proliferating regions of *Xrcc1*$^{Nes\text{-}cre}$ embryos (Suppl. Fig. 3a), while postnatal *Xrcc1*$^{Nes\text{-}cre}$ brain showed a progressive age-dependent accumulation of γH2AX foci (Fig. 3 and Suppl. Table 1). These γH2AX foci overlapped with those of another DNA damage marker, 53BP1 (Suppl. Fig. 3b), confirming there is widespread accumulation of DNA damage throughout the *Xrcc1*$^{Nes\text{-}cre}$ brain.

Xrcc1 deficiency leads to loss of cerebellar interneurons

Analysis of the *Xrcc1*$^{Nes\text{-}cre}$ brain revealed that most regions were generally similar to wild type brains. A survey of the *Xrcc1*$^{Nes\text{-}cre}$ central and peripheral nervous system, using various markers of differentiation, proliferation and apoptosis failed to find major consequences of Xrcc1 loss (Suppl. Fig. 4). However, exceptions to this were the cerebellum, which was proportionally smaller in the mutant animals (Fig. 4a) and the hippocampus (see later).

Histological analysis of the *Xrcc1*$^{Nes\text{-}cre}$ cerebellum revealed a profound and widespread loss of interneurons (Fig. 4b). These interneurons are critical for modulating the output of

the cerebellum, and function to attenuate granule and Purkinje cell electrical activity17, 18. Five different types of interneurons reside in the cerebellum; the stellate and basket cells in the molecular layer and Golgi cells in the granule cell layer (GCL), and the less abundant unipolar brush and Lugaro cells also found in the GCL17, 19-24. Cerebellar interneurons are GABAergic (γ-aminobutyric acid is used as a neurotransmitter), although unipolar brush cells are glutamatergic. Accordingly, we found that glutamic acid decarboxylase (the enzyme that catalyses synthesis of GABA) immunoreactivity in the molecular layer was almost absent in the *Xrcc1*$^{Nes\text{-}cre}$ cerebellum supporting a specific loss of basket and stellate cells (Fig. 4c). Furthermore, we found that the GCL displayed a substantial reduction of mGluR2, a metabotropic glutamate receptor present in Golgi cells, indicating an absence of this interneuron in the *Xrcc1*$^{Nes\text{-}cre}$ cerebellum (Fig. 4c). In contrast, unipolar brush and Lugaro cells in the mutant cerebellum were comparable to those of controls as judged by histology and immunohistochemistry (data not shown). Other cerebellar cell types including Purkinje cells (Fig. 4c), granule neurons and Bergmann glia (data not shown) appeared unaffected in the *Xrcc1*-deficient cerebellum. Furthermore, interneuron populations in other areas of the *Xrcc1*-deficient brain displayed normal neuronal organization, maturation and morphology (Suppl. Figs. 5 and 6). These data demonstrate that Xrcc1 has a critical role during genesis of basket, stellate and Golgi interneurons.

Interneuron progenitors are susceptible to Xrcc1 loss

Despite the pronounced effect of Xrcc1 loss on cerebellar neurogenesis, examination of embryonic neural development showed normal indices of proliferation (Ki67 and PCNA), differentiation (Tuj1) and maturation (NeuN) throughout the nervous system, including the embryonic cerebellum (Suppl. Figs. 7, 8 and 9). However, while neural progenitors were similar between controls and mutants as judged by Sox2 immunoreactivity, increased apoptosis was found in the *Xrcc1*$^{Nes\text{-}cre}$ proliferative ventricular zone (Suppl. Fig. 9), potentially contributing to an overall reduction in *Xrcc1*$^{Nes\text{-}cre}$ brain size.

The normal development of the *Xrcc1*$^{Nes\text{-}cre}$ embryonic cerebellum (Suppl. Fig. 8), suggested that Xrcc1 becomes particularly important as cerebellar interneuron progenitors begin to differentiate postnatally. Cerebellar interneurons originate from progenitors that reside in the white matter of the cerebellum and begin to differentiate around birth19, 20, 23, 25-28. To define the stage at which interneurons are susceptible to Xrcc1 loss we monitored interneuron progenitors using Pax220, 29. We also used Pax3 as a hindbrain marker, and as an adjunct to Pax2 for identifying immature cerebellar interneurons. Compared with wild type tissue, there was a striking reduction of Pax2-positive interneuron progenitors in the *Xrcc1*$^{Nes\text{-}cre}$ cerebellum from P0 onwards (Fig. 5a,b and Suppl. Fig. 10). We observed a similar absence of Pax3 positive cells from the *Xrcc1*$^{Nes\text{-}cre}$ white matter, while in contrast abundant Pax3 positive cells were present in the wild type tissue (Fig. 5b,c). Pax3 also marks granule neuron progenitors (GNPs) in the external germinal layer (EGL). Pax3 and PCNA positive cells were also found in the EGL of both mutants and controls, indicating that this region is substantially less affected by Xrcc1 loss (Fig. 5b,c). These data indicate that the interneuron defect in the *Xrcc1*$^{Nes\text{-}cre}$ cerebellum is the result of a selective loss of differentiating interneuron progenitors, and that this occurs early in postnatal cerebellar

development. However, because defects are noticeable from P0 onwards, the actual impact of Xrcc1 loss upon the interneuron progenitors likely occurs prior to P0.

Interneuron progenitors undergo p53-dependent arrest

The loss of interneuron progenitor cells in the *Xrcc1*$^{Nes\text{-}cre}$ white matter could result from either DNA damage-induced cell cycle arrest or apoptosis. We confirmed that interneuron progenitor cells in the *Xrcc1*$^{Nes\text{-}cre}$, but not matched controls, accumulated γH2AX foci, indicative of DNA damage (Fig. 6a). We then determined levels of cellular proliferation in various regions of the developing cerebellum using PCNA and BrdU, compared with levels of apoptosis. The *Xrcc1*$^{Nes\text{-}cre}$ white matter showed a marked decrease in proliferating cells relative to control tissue (Fig. 6b). In contrast, *Xrcc1*$^{Nes\text{-}cre}$ white matter did not show levels of apoptosis beyond those in the control cerebellum (Fig. 6b), nor was increased apoptosis seen at any day between P0 through P10, or in the embryonic cerebellum (not shown). However, apoptosis was high in the *Xrcc1*$^{Nes\text{-}cre}$ EGL as determined by TUNEL and caspase-3 activation (Fig. 6c,d), highlighting the distinct outcomes after DNA damage in different cell types. Moreover, we found increased p53 levels and concomitant increased immunoreactivity of the cyclin dependent kinase inhibitors p21 and p27 within the cerebellar white matter, but not the EGL (Fig. 6e), suggesting that cell cycle arrest, rather than apoptosis, accounts for the loss of interneurons in the *Xrcc1*$^{Nes\text{-}cre}$ cerebellum.

Due to the prominent role of p53-mediated signaling after DNA damage in the developing nervous system30, we generated *Xrcc1*$^{Nes\text{-}cre}$*;p53*$^{-/-}$ animals to assess the contribution of p53 towards interneuron loss. We found a complete rescue of interneurons in the molecular layer of the *Xrcc1*$^{Nes\text{-}cre}$*;p53*$^{-/-}$ cerebellum, reflected by a normal distribution of basket and stellate cells (Fig. 7). These interneurons retained many functional properties, as they were immunopositive for parvalbumin, superoxide dismutase 2 and GAD, and synapsed extensively with Purkinje dendrites (Fig. 7 and Suppl. Fig. 6 and 11). However, Golgi cells within the GCL of the cerebellum were only partially rescued (Fig. 7, asterisk), suggesting a particular susceptibility to genotoxic stress, possibly reflecting the earlier genesis and unique identity of the Golgi interneurons20, 23. It is noteworthy that only complete inactivation of p53 rescues the interneuron phenotype, not p53 heterozygosity (Fig. 7 and Suppl. Fig. 11), as it does when apoptosis is the end point of DNA damage in the developing nervous system30.

Xrcc1$^{Nes\text{-}cre}$*;p53*$^{-/-}$ animals also rapidly developed medulloblastoma brain tumors (Suppl. Fig. 12). Some *Xrcc1*$^{Nes\text{-}cre}$*;p53*$^{+/-}$ animals (12.5%, 3/24) also developed medulloblastoma after loss of the wildtype *p53* allele (Suppl. Fig. 12 and data not shown). Comparative analysis of Xrcc1-deficient medulloblastoma with other medulloblastoma models from our laboratory, showed a similar cytogenetic and expression array profile (data not shown), indicating that this tumor originated from the GNPs of the EGL11, 31, 32. This was further confirmed by interbreeding *Xrcc1*$^{Nes\text{-}cre}$*;p53*$^{+/-}$ with a mouse engineered to express green fluorescent protein from the *Math1* promoter33, which is highly expressed in the GNPs (Suppl. Fig. 12).

Thus, Xrcc1 loss results in two unique outcomes in the cerebellum in response to genotoxic stress. Within the white matter, Xrcc1 is necessary in neuroprogenitors to suppress DNA

damage-induced p53-mediated cell cycle checkpoint activation. In contrast, Xrcc1 loss in the EGL leads to DNA damage-induced p53-mediated apoptosis.

Xrcc1 deficiency affects hippocampal function

Xrcc1$^{Nes\text{-}cre}$ adult mice displayed a behavioral phenotype consistent with either seizure or episodic epilepsy (Suppl. Movie). A brain region often associated with this type of behavioral deficit is the hippocampus34. We found no differences in the general cellularity between the control and mutant hippocampus (Suppl. Figs. 5 and 7a), although increased DNA damage (γH2AX foci) was present in *Xrcc1*$^{Nes\text{-}cre}$ tissue (Fig. 3 and 8a and Suppl. Fig. 3). A marked reduction in the levels of the Xrcc1-binding protein Parp1 was also found in the *Xrcc1*$^{Nes\text{-}cre}$ hippocampus (Fig. 8a), indicating that loss of Xrcc1 in this tissue may further destabilize components of the SSBR pathway.

Consistent with a seizure phenotype, we found features common to temporal lobe epilepsy35 in the *Xrcc1*$^{Nes\text{-}cre}$ hippocampus such as abnormally high levels of neuropeptide Y (NPY) and evidence of gliosis, such as increased levels of glial fibrillary acidic protein and vimentin (Fig. 8b). *Xrcc1*-deficient hippocampal neurons also showed abnormal activity as revealed by increased c-Fos immunoreactivity36 and a specific reduction of the oligodendrocyte marker 2,3-Cyclic Nucleotide 3-Phosphodiesterase (CNPase). These results indicate that Xrcc1 is required for hippocampal homeostasis.

DISCUSSION

DNA repair is an essential feature of neural development, and defects in this process can result in human neurological disease1-3. For example, defects in the DNA SSBR end-processing enzymes APTX and TDP1, which are required for the repair of specific DNA lesions, are associated with the neurodegenerative syndromes AOA1 and SCAN1 respectively. Although these syndromes illustrate the need for maintaining genomic integrity, they do not fully elaborate the requirements for the DNA SSBR pathway during neural development. Therefore, we inactivated the central DNA SSBR factor Xrcc1 to assess the role of this repair pathway during CNS development.

While inactivation of Xrcc1 throughout the nervous system markedly affected the cerebellar interneurons and the hippocampus, there was also a progressive accumulation of persistent DNA strand breaks throughout the brain. A general increase in apoptosis in the neuroepithelia was also observed throughout neural development and likely accounts for the smaller brain size found in the *Xrcc1*$^{Nes\text{-}cre}$ animals. Our findings illustrate the central importance of this DNA repair pathway during genesis of the nervous system, and highlight cerebellar interneurons as a heretofore-unrecognized target of defective DNA repair. This is particularly noteworthy as the cerebellum is often affected in human neurological disease resulting from DNA repair deficiency37. It will be important to further investigate these diseases to determine to what extent interneurons are involved in the resulting neuropathology.

The cerebellum is a laminar structure containing three main layers, the GCL, the Purkinje cell layer and the molecular layer18, 38, 39. Stellate and basket interneurons reside in the

molecular layer, while the Golgi cells and other interneurons (the less common unipolar brush cells and Lugaro cells) reside in the GCL18, 40. Purkinje cells are the primary output from the cerebellum. Parallel fiber projections from granule neurons make synaptic contact with Purkinje cell dendrites, and also provide excitatory contact with the Golgi, stellate and basket cells. In turn, the stellate and basket cells make inhibitory contact with the Purkinje cells to modulate signaling to the deep cerebellar nuclei17, 18, 39, 40. Therefore, interneurons are integral to cerebellar function and play an important role in modulating Purkinje and granule cell output in the cerebellum. Notably, selective ablation of Golgi cells can result in profound cerebellar dysfunction21.

Our data demonstrates for the first time that Xrcc1 is critical for the formation of cerebellar interneurons. These interneurons form postnatally from migrating progenitor cells in the white matter of the cerebellum23, 26, 28, 41. To determine the mechanism of interneuron loss, we surveyed embryonic and postnatal cerebellar development in *Xrcc1*$^{Nes\text{-}cre}$ animals to identify when interneuron progenitors are susceptible to Xrcc1 loss. We found that interneuron loss coincided with a failure of progenitor cell proliferation and differentiation from around P0 onwards. At this stage, DNA damage accumulated in *Xrcc1*$^{Nes\text{-}cre}$ progenitors leading to an increase in the cyclin dependent kinase inhibitors p21 and p27, reflective of activation of a p53-dependent cell cycle checkpoint.

It is well established that apoptosis and cell cycle arrest are alternative outcomes of DNA damage42, and our data indicate that within the cerebellum specific cell types respond differently to DNA damage. We showed that the granule neurons of the EGL undergo DNA damage-induced apoptosis, while interneuron progenitors respond to DNA damage via a p53-dependent cell cycle arrest. Xrcc1 loss impacts this progenitor population postnatally as they commence differentiation. Before this stage, homologous recombination is available as a backup system for DNA repair5 and may partially compensate for Xrcc1 loss. Other studies indicate that interneurons can be affected by perturbations in proliferation control, as cyclin D2-null mice develop a cerebellum essentially devoid of stellate interneurons, suggesting a specific regulation of cell fate as these progenitors differentiate43, 44.

In addition to the cerebellum, the hippocampus was also affected by Xrcc1 inactivation. Although there was no overt cell loss, *Xrcc1*$^{Nes\text{-}cre}$ hippocampal neurons showed DNA damage and associated neuropathology as indicated by gliosis, and elevated c-Fos levels. These features resemble the neuropathology of temporal lobe epilepsy, a frequent type of epilepsy in human adults with seizure as a primary clinical manifestation35. Similarly, adult *Xrcc1*$^{Nes\text{-}cre}$ animals exhibited sporadic seizure-like activity. Perhaps the high levels of NPY found in the *Xrcc1*$^{Nes\text{-}cre}$ hippocampus and its anti-epileptic functions reflects an attempt to counteract uncontrolled neuronal activity and seizure45, 46.

Mature neurons throughout the *Xrcc1*-deficient brain accumulate DNA damage with age. Because persistent γH2AX and 53BP1 foci usually denote DNA DSBs and not SSBs, it is surprising these are found in the mature *Xrcc1*$^{Nes\text{-}cre}$ brain. This may indicate that γH2AX foci reflect the rapid *in vivo* accumulation of DNA SSBs whereby adjacent breaks are sensed as DNA DSBs. While the link between Xrcc1 and DNA DSB repair is unclear47, we did not find defects in DSBR in *Xrcc1*$^{Nes\text{-}cre}$ neural cells, based on γH2AX recovery assays after IR

(not shown). Additionally, it is also surprising that if Xrcc1 loss does lead to DNA DSBs that NHEJ does not repair the damage12; particularly since recovery of IR-induced γH2AX in the *Xrcc1*$^{Nes\text{-}cre}$ brain occurs with normal kinetics (data not shown). Alternatively, γH2AX foci can reflect structural changes in chromatin other than the formation of a DSB, which might occur by persistent DNA repair factor association with chromatin48. Perhaps then, the progressive accumulation of γH2AX in the *Xrcc1*$^{Nes\text{-}cre}$ brain reflects the slow repair of SSBs, and prolonged accumulation of repair factors at the break that modify chromatin structure.

Collectively, our data has shown that DNA SSBR is critical for neural development and that this pathway is essential for the genesis of cerebellar interneurons and hippocampal function. These data will be important for understanding the role the DNA damage response plays in preventing neurological disease.

EXPERIMENTAL PROCEDURES

Generation of *Xrcc1* conditional knockout animal model

To generate the *Xrcc1* conditional allele, we obtained a mouse BAC containing the *Xrcc1* locus (Invitrogen), and cloned a 9.8 Kb NcoI genomic fragment containing exons 4 to 14 of the *Xrcc1* gene into pBluescript II (Stratagene). An oligo containing a *LoxP* site was introduced into a BglII site located between exons 12 and 13. A Neomycin-thymidine kinase (Neo-TK) cassette flanked by *LoxP* sites was then inserted into a SpeI site located upstream of exon 4. Targeted W9.5 embryonic stem (ES) cells were selected using G418 followed by removal of a Neo-TK cassette using *pMC-Cre* and then selection in FIAU (1-(2-deoxy-2-fluoro-1-D-arabinofuranosyl)-5-iodouracil)-containing media. ES targeting was confirmed by Southern blot analysis of Nhe1 and Xba1 digested genomic DNA using a 3′ probe amplified by PCR using the following primers; forward-5′ TTA GCT ACT GCT TAG CAC CAG GC and reverse-3′ GCA GCT GCC TGT GAG ACC TGT GC (blue bar in Suppl. Fig. 1a). Southern blot analysis with this probe yields a 5.8 kb fragment in wildtype ES genomic DNA, while sizes are 3.4 kb in floxed and 4 kb in knockout genomic DNA (Suppl. Fig. 1b). Male chimeras generated after blastocyst injection of targeted ES cells were bred with C57BL/6 females to identify germline transmission, and then used to generate animals carrying the floxed *Xrcc1* gene (*Xrcc1*$^{LoxP/+}$).

In order to inactivate the *Xrcc1* gene in the nervous system, we interbred *Xrcc1*$^{LoxP/+}$ mice with *Nestin-cre* mice (B6.Cg-Tg(Nes-cre)1Kln/J, JAX #003771). *Xrcc1*$^{LoxP/LoxP}$*;Nestin-cre* animals were obtained by crossing male *Xrcc1*$^{LoxP/LoxP}$ or *Xrcc1*$^{LoxP/+}$ and female *Xrcc1*$^{LoxP/+}$*;Nestin-cre*. We maintained *Nestin-cre* maternally to restrict ectopic cre recombinase activity in the testis. Meox2-cre (B6.129S4-*Meox2tm1(cre)Sor*/J, JAX # 003755) was used to delete Xrcc1 in the epiblast layer to determine the consequence of gene deletion in the embryo without placental gene inactivation. Importantly, mice with floxed *Xrcc1* alleles (*Xrcc1*$^{LoxP/LoxP}$) were identical to littermate controls (*Xrcc1*$^{LoxP/+}$ or *Xrcc1*$^{+/+}$) indicating that the *LoxP* sites did not affect Xrcc1 function. Mice carrying only *Meox2-cre* or *Nestin-cre* were also indistinguishable from wild type mice. *Math1-GFP* mice33 were kindly provided by Dr. Jane Johnson (UT Southwestern).

Genotypes of animals were determined by PCR. For the *Xrcc1* gene, the following three primers were used (red bars in Suppl. Fig. 1a); PC1-5′ TAT GCT TGC TGT ACA GGG ATT GGG C, PC2-5′ TGG ACC ATG AAA AAG CTG TGT GC and PC4-5′ GTC CTC ACT GCT GGA TCC AAG G. PCR with a combination of primers PC1 and PC2 discriminates wildtype (245 bp) and floxed *Xrcc1* gene (279 bp), whereas PC1/4 PCR produces a detectable fragment (274 bp) when the targeted portion of the *Xrcc1* gene is deleted. PCR products were amplified for 35 cycles of 94°C for 30 seconds, 59°C for 45 seconds and 72°C for 45 seconds. *Cre* recombinase was detected using the following primers and PCR conditions; Cre-3-5′ CTG CCA CGA CCA AT GAC AGC and Cre-4-5′ ACC TGC GGT GCT AAC CAG CG for 35 cycles of 94°C for 30 seconds, 60°C for 45 seconds, and 72°C for 45 seconds.

The presence of a vaginal plug was designated as embryonic day 0.5 (E0.5) and the day of birth as postnatal day 0 (P0). All animals were housed in an AAALAC-accredited facility and were maintained in accordance with the NIH *Guide for the Care and Use of Laboratory Animals*. All procedures involving animals were approved by the St. Jude Children's Research Hospital institutional animal care and use committee.

Generation of Xrcc1 antibody and Western blot analysis

A rabbit polyclonal antibody against Xrcc1 was generated using a 15-residue peptide (NH_2-AEDSGDTEDELRRVA) corresponding to aa481-495 of murine Xrcc1. Western blot analysis was done using 3-week old neural (cortex and cerebella) and extra-neural (spleen and thymus) whole tissue extracts from control (*Xrcc1*$^{LoxP/+}$*;Nestin Cre*) and conditional knockout mice (*Xrcc1*$^{LoxP/LoxP}$*;Nestin Cre*). Protein extracts were prepared in lysis buffer (50mM Tris-HCl, 200mM NaCl, 0.2% NP-40, 1% Tween-20, 1mM NaF, 1mM sodium vanadate, 50mM β-glycerophosphate, 2mM PMSF, 1x Complete-EDTA (Roche)) and quantified by Bradford assay (Bio-Rad). Proteins (50μg/lane) were separated through a 4-12% Bis-Tris SDS poly-acrylamide gel (Invitrogen) and transferred onto nitrocellulose membrane (Bio-Rad). Blots were sequentially immunostained with affinity-purified rabbit polyclonal anti-Xrcc1 (1:1000) followed by horseradish peroxidase-conjugated donkey anti-rabbit secondary antibody (1:2000; GE Healthcare) and detected using ECL Plus chemiluminescence reagent (GE Healthcare). To assess Ligase 3 protein levels, immunoblots were stained with mouse anti-Lig3 antibody (1:200; BD) and processed as above. Actin antibody (1:750; Santa Cruz Biotech) served as a protein-loading control.

Histology

Embryos and brain tissues were removed at indicated ages after transcardial pefusion with 4% buffered paraformaldehyde and for cryosectioning were cryoprotected in buffered 25% sucrose solution and sectioned at 10μm using an HM500M cryostat (Microm). Alternatively, tissues were fixed in 10% buffered formalin, embedded in paraffin, and sectioned at 7μm using an HM325 microtome (Microm). Nissl staining was done with 1% thionin. Hematoxylin and Eosin staining was done according to standard procedures.

Immunohistochemical and immunocytochemical analysis of tissues and cells respectively were performed using the antibodies listed below. For colorimetric visualization of positive

signals, sections were incubated with antibodies overnight after quenching endogenous peroxidase using 0.6% H_2O_2 in methanol. After washing slides with PBS several times, the tissues were treated with biotinylated secondary antibody and Avidin-Biotin complex (Vectastain Elite kit, Vector Labs). Immunoreactivity was visualized with the VIP substrate kit (Vector Labs) according to the manufacturer's protocol. Sections were counterstainined with 0.1% methyl green, dehydrated, and mounted in DPX (Fluka). For fluorescent signals of immunoreactivity, FITC or Cy3 conjugated secondary antibodies (Jackson Immunologicals) were used, and counterstained with DAPI or PI (Vector Laboratories).

For BrdU incorporation studies, P7 brains were removed 2 hours after BrdU injection (60μg/g b.w., i.p. injection). Apoptosis was measured by immunoreactivity to ssDNA antibody (IBL International GmbH) and TUNEL assays using Apoptag (Chemicon) according to the manufacturer's protocol. All stained slides were examined and imaged using an Axio Imager A1 microscope (Zeiss), and captured and processed using Adobe Photoshop.

Antibodies

The following antibodies were used for immunohistochemistry or immunocytochemistry: β–tubulin III (clone Tuj1, mouse, 1:1000, BabCo), Calbindin-D28K (mouse, 1:2000, Sigma), Calretinin (mouse, 1:1000, Chemicon), GABA receptor α6 (rabbit, 1:500, Chemicon), GFAP (mouse, 1:400, Sigma, and rabbit, 1:200, Abcam), Pax2 (rabbit, 1:500, Zymed), Pax3 (rabbit, 1:500, a generous gift from Dr. Gerard Grosveld at St. Jude Children's Hospital), Superoxide dismutase 2 (rabbit, 1:500, Stressgen), Somatostatin (rabbit, 1:2000, ImmunoStar Inc.), Synaptophysin (mouse, 1:1000, Chemicon), BrdU (rat, 1:200, Abcam), γH2AX (rabbit, 1:500, abcam), 53BP1 (rabbit, 1:500, Bethyl Laboratories), Ki67 (rabbit, 1:2500, Vector Laboratories), Parvalbumin (Guinea Pig, 1:1000, Chemicon), p21 (mouse, 1:100, Santa Cruz Biotechnology), p53 (CM5) (rabbit, 1:1000, Vector Laboratories), p27 (rabbit, 1:100, Santa Cruz Biotechnology), Parp1 (rabbit, 1:25, Abcam, and mouse, 1:50, Novus) and PCNA (mouse, 1:500, Santa Cruz Biotechnology). Antibodies listed above were used with citrate buffer-based antigen retrieval treatment.

The following antibodies were used without antigen retrieval: c-Fos (K-25, rabbit, 1:1000, Santa Cruz Biotechnology), CNPase (2,3-Cyclic Nucleotide 3-Phosphodiesterase, mouse, 1:500, Sigma), GAD67 (rabbit, 1:500, Chemicon), mGluR2 (rabbit, 1:500, Upstate), Neu N (mouse, 1:500, Chemicon), NPY (neuropeptide Y, rabbit, 1:5000, Novus), Vimentin (mouse, clone RV202, 1:200, Abcam), ssDNA (rabbit, 1:300, IBL), and actin (goat, 1:1000, Santa Cruz Biotechnology).

Isolation of primary mouse granule cell neurons and astrocytes

Cerebellar granule cells were purified from P7 brains49; whole cerebella were treated with low activity (1:250) trypsin (Gibco)-DNAse I (Worthington) and triturated with Pasteur pipettes into a single-cell suspension. The cell suspension was applied to a Percoll (GE Healthcare) gradient (35%/60%) and separated by centrifugation (1200g). Enriched granule cell neurons were grown in neural basal medium (Gibco) supplemented with 1x glutamax, 100U/ml penicillin, 100μg/ml streptomycin, 2% D+Glucose (Sigma), 1x SPITE (Sigma), 1x

Oleic acid albumin/linoleic acid (Sigma), and 16μg/ml *N*-Acetyl Cysteine (Sigma) on poly-D-lysine-/matrigel-coated (Gibco and Becton Dickson, respectively) glass-bottom multi-chamber slides (Falcon) at a density of 3×10^5 cells/well. For *in vivo* comet assays, cells from P15 cerebella were subjected to alkali comet analysis (ACA) directly upon Percoll-mediated enrichment. Immunofluorescent staining of granule cell neurons was performed as previously described50 using anti-Tuj1 (β-tubulin III; 1:500) and phalloidin (1:500; Molecular Probes).

Primary murine astrocytes were prepared from P3 brains as described50. Cortices were dissociated by passage through a 5 ml pipette and cells were resuspended in Dulbecco's modified Eagle's medium and Ham's nutrient mixture F-12 (1:1 DMEM/F12; Gibco-BRL) supplemented with 10% fetal bovine serum, 1x glutamax, 100U/ml penicillin, 100μg/ml streptomycin, and 20ng/ml epidermal growth factor (Sigma). Primary astrocytes were established in Primeria T-25 tissue culture flasks (Falcon) at 37°C in a humidified oxygen-regulated (9%) incubator. Culture medium was changed after 3 days and astrocyte monolayers reached confluence 3 days later.

Alkaline comet assay (ACA)

Primary granule cell neurons or quiescent primary murine astrocytes (3×10^5 cells/ml/sample) were treated with either 100μM (neurons), 150μM (astrocytes) H_2O_2 for 10 mins on ice, methyl methanesulfonate (MMS) for 10 mins at various concentrations or γ-irradiation (20Gy; cesium^{137}). Cells were then incubated for various times in drug-free medium at 37°C. Cells were suspended in pre-chilled PBS and mixed with equal volume of 1.2% low-melting point (LMP) agarose (Invitrogen) maintained at 42°C, and then immediately layered onto frosted glass slides (Fisher) pre-coated with 0.6 % agarose, and maintained in the dark at 4°C for all further steps. Slides were immersed in pre-chilled lysis buffer (2.5M NaCl, 10mM Tris-HCl, 100mM EDTA pH 8.0, 1% Triton X-100, 3% DMSO; pH10) for 1 hour, washed with pre-chilled distilled water (2 × 10 mins), and placed for into pre-chilled alkaline electrophoresis buffer (50mM NaOH, 1mM EDTA, 1% DMSO) for 45 mins. Electrophoresis was at 95mA for 25 mins, followed by neutralization in 0.4M Tris-HCl pH 7.0. Comets were stained with SYBR Green (1:10,000 in PBS, SIGMA) for 10 mins. A minimum of 50 comet tail moments were measured using the Comet Assay IV system (Perceptive Instruments, UK) coupled to an Axioskop2 plus microscope (Zeiss) at 200x magnification.

MRI and Statistical analysis

Adult mutant and control animals (age and sex matched) were subject to magnetic resonance imaging (MRI) analysis. All subjects were scanned on a 7 Tesla Bruker Clinscan animal MRI scanner (Bruker BioSpin MRI GmbH, Germany) using the Bruker 12S gradient BGA12S and the 4 channel mouse surface coil (for T2 weighted images in two directions: in the sagittal scan, matrix = 320 × 320, field of view (FOV) = 25 × 25 mm, slices = 17 contiguous, thickness = 0.7 mm, echo time (TE) = 39 ms, repetition time (TR) = 2579 ms / in the axial scan, matrix = 320 × 320, field of view (FOV) = 25 × 25 mm, slices = 16 contiguous, thickness = 0.5 mm, echo time (TE) = 42 ms, repetition time (TR) = 2620 ms). The volumetric measurement of the brain was performed using ImageJ (v1.41n, NIH). For

quantification analysis of cell cycle and cell death, immunopositive cells in the EGL, IGL, WM and DN within 1μm^2 of the lingual and lobulus centralis in the cerebellum at P7 were counted in at least 6 representative sections and mean values were calculated and statistically analyzed. These data were collected from 3 different animals per each group. All statistical analyses were performed using Prism (v4.0, Graphpad), and differences were considered significant when P value was < 0.05.

Supplementary Material

Refer to Web version on PubMed Central for supplementary material.

ACKNOWLEDGEMENTS

We thank the Hartwell Center for biotech support, the Transgenic core facility for blastocyst injections, the Animal Imaging core for MRI analysis and Jingfeng Zhao for genotyping. P.J.M is supported by the NIH (NS-37956 and CA-21765), the CCSG (P30 CA21765) and the American Lebanese and Syrian Associated Charities of St. Jude Children's Research Hospital. K.W.C is supported by the Medical Research Council (Grants G0600776 & G0400959) and by the EU Integrated Project on DNA Repair. S.K. is a Neoma Boadway AP Endowed Fellow and S.E.K is supported by the Wellcome Trust (Grant 085284).

References

1. McKinnon PJ. DNA repair deficiency and neurological disease. Nature Reviews Neurosci. 2009; 10:100–112.
2. McKinnon PJ, Caldecott KW. DNA strand break repair and human genetic disease. Annu Rev Genomics Hum Genet. 2007; 8:37–55. [PubMed: 17887919]
3. Rass U, Ahel I, West SC. Defective DNA repair and neurodegenerative disease. Cell. 2007; 130:991–1004. [PubMed: 17889645]
4. Ahel I, et al. The neurodegenerative disease protein aprataxin resolves abortive DNA ligation intermediates. Nature. 2006; 443:713–716. [PubMed: 16964241]
5. El-Khamisy SF, et al. Defective DNA single-strand break repair in spinocerebellar ataxia with axonal neuropathy-1. Nature. 2005; 434:108–113. [PubMed: 15744309]
6. Moreira MC, et al. The gene mutated in ataxia-ocular apraxia 1 encodes the new HIT/Zn-finger protein aprataxin. Nat Genet. 2001; 29:189–193. [PubMed: 11586300]
7. Takashima H, et al. Mutation of TDP1, encoding a topoisomerase I-dependent DNA damage repair enzyme, in spinocerebellar ataxia with axonal neuropathy. Nat Genet. 2002; 32:267–272. [PubMed: 12244316]
8. Tebbs RS, et al. Requirement for the Xrcc1 DNA base excision repair gene during early mouse development. Dev Biol. 1999; 208:513–529. [PubMed: 10191063]
9. Tallquist MD, Soriano P. Epiblast-restricted Cre expression in MORE mice: a tool to distinguish embryonic vs. extra-embryonic gene function. Genesis. 2000; 26:113–115. [PubMed: 10686601]
10. Caldecott KW. DNA single-strand break repair and spinocerebellar ataxia. Cell. 2003; 112:7–10. [PubMed: 12526788]
11. Frappart PO, Lee Y, Lamont J, McKinnon PJ. BRCA2 is required for neurogenesis and suppression of medulloblastoma. Embo J. 2007; 26:2732–2742. [PubMed: 17476307]
12. Shull ER, et al. Differential DNA damage signaling accounts for distinct neural apoptotic responses in ATLD and NBS. Genes Dev. 2009; 23:171–180. [PubMed: 19171781]
13. Caldecott KW, McKeown CK, Tucker JD, Ljungquist S, Thompson LH. An interaction between the mammalian DNA repair protein XRCC1 and DNA ligase III. Mol Cell Biol. 1994; 14:68–76. [PubMed: 8264637]
14. Kulkarni A, McNeill DR, Gleichmann M, Mattson MP, Wilson DM 3rd. XRCC1 protects against the lethality of induced oxidative DNA damage in nondividing neural cells. Nucleic Acids Res. 2008; 36:5111–5121. [PubMed: 18682529]

15. Rogakou EP, Pilch DR, Orr AH, Ivanova VS, Bonner WM. DNA double-stranded breaks induce histone H2AX phosphorylation on serine 139. J Biol Chem. 1998; 273:5858–5868. [PubMed: 9488723]
16. Sedelnikova OA, Pilch DR, Redon C, Bonner WM. Histone H2AX in DNA damage and repair. Cancer Biol Ther. 2003; 2:233–235. [PubMed: 12878854]
17. Barmack NH, Yakhnitsa V. Functions of interneurons in mouse cerebellum. J Neurosci. 2008; 28:1140–1152. [PubMed: 18234892]
18. Sillitoe RV, Joyner AL. Morphology, molecular codes, and circuitry produce the three-dimensional complexity of the cerebellum. Annu Rev Cell Dev Biol. 2007; 23:549–577. [PubMed: 17506688]
19. Eccles JC. Neurogenesis and morphogenesis in the cerebellar cortex. Proc Natl Acad Sci U S A. 1970; 66:294–301. [PubMed: 4915885]
20. Weisheit G, et al. Postnatal development of the murine cerebellar cortex: formation and early dispersal of basket, stellate and Golgi neurons. Eur J Neurosci. 2006; 24:466–478. [PubMed: 16903854]
21. Watanabe D, et al. Ablation of cerebellar Golgi cells disrupts synaptic integration involving GABA inhibition and NMDA receptor activation in motor coordination. Cell. 1998; 95:17–27. [PubMed: 9778244]
22. Englund C, et al. Unipolar brush cells of the cerebellum are produced in the rhombic lip and migrate through developing white matter. J Neurosci. 2006; 26:9184–9195. [PubMed: 16957075]
23. Yamanaka H, Yanagawa Y, Obata K. Development of stellate and basket cells and their apoptosis in mouse cerebellar cortex. Neurosci Res. 2004; 50:13–22. [PubMed: 15288494]
24. Weyer A, Schilling K. Developmental and cell type-specific expression of the neuronal marker NeuN in the murine cerebellum. J Neurosci Res. 2003; 73:400–409. [PubMed: 12868073]
25. Rakic P. Kinetics of proliferation and latency between final cell division and onset of differentiation of cerebellar stellate and basket neurons. J Comp Neurol. 1973; 147:523–546. [PubMed: 4122708]
26. Lee A, et al. Isolation of neural stem cells from the postnatal cerebellum. Nat Neurosci. 2005; 8:723–729. [PubMed: 15908947]
27. Kenney AM, Segal RA. Subtracting the Math: prominin-positive cerebellar stem cells in white matter. Nat Neurosci. 2005; 8:699–701. [PubMed: 15917830]
28. Zhang L, Goldman JE. Generation of cerebellar interneurons from dividing progenitors in white matter. Neuron. 1996; 16:47–54. [PubMed: 8562089]
29. Maricich SM, Herrup K. Pax-2 expression defines a subset of GABAergic interneurons and their precursors in the developing murine cerebellum. J Neurobiol. 1999; 41:281–294. [PubMed: 10512984]
30. Lee Y, McKinnon PJ. Responding to DNA double strand breaks in the nervous system. Neuroscience. 2007; 145:1365–1374. [PubMed: 16934412]
31. Lee Y, McKinnon PJ. DNA ligase IV suppresses medulloblastoma formation. Cancer Res. 2002; 62:6395–6399. [PubMed: 12438222]
32. Orii KE, Lee Y, Kondo N, McKinnon PJ. Selective utilization of nonhomologous end-joining and homologous recombination DNA repair pathways during nervous system development. Proc Natl Acad Sci U S A. 2006; 103:10017–10022. [PubMed: 16777961]
33. Lumpkin EA, et al. Math1-driven GFP expression in the developing nervous system of transgenic mice. Gene Expr Patterns. 2003; 3:389–395. [PubMed: 12915300]
34. McNamara JO, Huang YZ, Leonard AS. Molecular signaling mechanisms underlying epileptogenesis. Sci STKE. 2006; 2006:re12. [PubMed: 17033045]
35. Aronica E, Gorter JA. Gene expression profile in temporal lobe epilepsy. Neuroscientist. 2007; 13:100–108. [PubMed: 17404370]
36. Morgan JI, Cohen DR, Hempstead JL, Curran T. Mapping patterns of c-fos expression in the central nervous system after seizure. Science. 1987; 237:192–197. [PubMed: 3037702]
37. Frappart PO, McKinnon PJ. Ataxia-telangiectasia and related diseases. Neuromolecular Med. 2006; 8:495–511. [PubMed: 17028372]

38. Goldowitz D, Hamre K. The cells and molecules that make a cerebellum. Trends Neurosci. 1998; 21:375–382. [PubMed: 9735945]
39. Wang VY, Zoghbi HY. Genetic regulation of cerebellar development. Nature Reviews Neurosci. 2001; 2:484–491.
40. Sotelo C. Cellular and genetic regulation of the development of the cerebellar system. Prog Neurobiol. 2004; 72:295–339. [PubMed: 15157725]
41. Leto K, Carletti B, Williams IM, Magrassi L, Rossi F. Different types of cerebellar GABAergic interneurons originate from a common pool of multipotent progenitor cells. J Neurosci. 2006; 26:11682–11694. [PubMed: 17093090]
42. Kastan MB, Bartek J. Cell-cycle checkpoints and cancer. Nature. 2004; 432:316–323. [PubMed: 15549093]
43. Glickstein SB, et al. Selective cortical interneuron and GABA deficits in cyclin D2-null mice. Development. 2007; 134:4083–4093. [PubMed: 17965053]
44. Huard JM, Forster CC, Carter ML, Sicinski P, Ross ME. Cerebellar histogenesis is disturbed in mice lacking cyclin D2. Development. 1999; 126:1927–1935. [PubMed: 10101126]
45. Howell OW, et al. Neuropeptide Y is important for basal and seizure-induced precursor cell proliferation in the hippocampus. Neurobiol Dis. 2007; 26:174–188. [PubMed: 17317195]
46. Baraban SC. Neuropeptide Y and epilepsy: recent progress, prospects and controversies. Neuropeptides. 2004; 38:261–265. [PubMed: 15337378]
47. Caldecott KW. XRCC1 and DNA strand break repair. DNA Repair (Amst). 2003; 2:955–969. [PubMed: 12967653]
48. Soutoglou E, Misteli T. Activation of the Cellular DNA Damage Response in the Absence of DNA Lesions. Science. 2008
49. Hatten ME. Neuronal regulation of astroglial morphology and proliferation in vitro. J Cell Biol. 1985; 100:384–396. [PubMed: 3881455]
50. Katyal S, et al. TDP1 facilitates chromosomal single-strand break repair in neurons and is neuroprotective in vivo. Embo J. 2007; 26:4720–4731. [PubMed: 17914460]

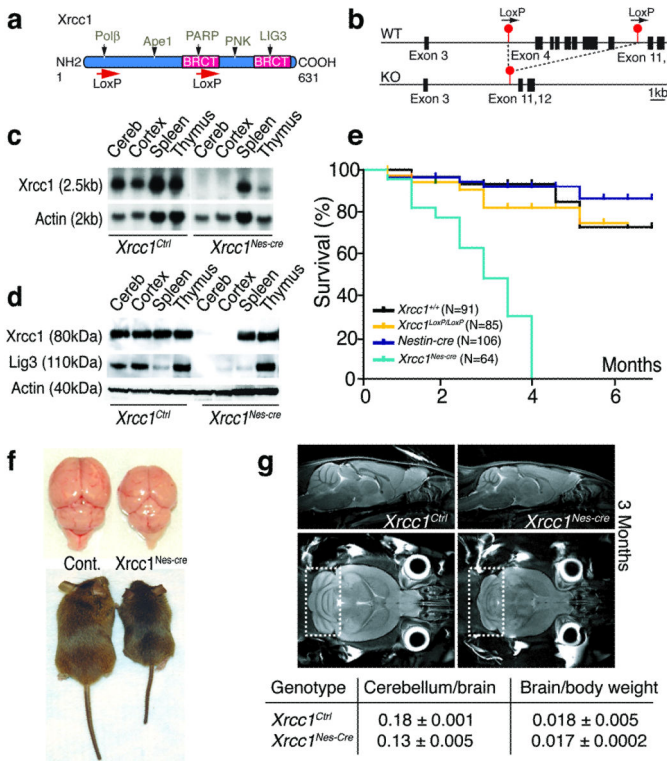

Figure 1. Generation of an *Xrcc1* conditional mouse

(**a**) Schematic diagram of Xrcc1 indicating BRCT (BRCA1-related C-terminal) domains and the regions associated with DNA repair protein interactions. (**b**) The *Xrcc1*-targeting construct was engineered with *LoxP* sites flanking exons 4 to 10 (specific details are provided in Suppl. Fig. 1a). (**c**) Northern blot analysis indicates control animals produce an *Xrcc1* transcript (2.5 kb) while an *Xrcc1* transcript is absent in the $Xrcc1^{Nes\text{-}cre}$ cerebellum and cerebral cortex. Actin mRNA (2 kb) served as a loading control. (**d**) Western blot analysis indicates that Xrcc1 protein (~80 kDa) is absent from the $Xrcc1^{Nes\text{-}cre}$ brain and this is associated with a decrease in levels of the Xrcc1-associated protein DNA Ligase 3 (~110 kDa). In contrast, spleen and thymus of the $Xrcc1^{Nes\text{-}cre}$ animals produced comparable amounts of Xrcc1 and Ligase 3 to those of controls. Actin was used as a loading control. (**e**) Kaplan-Meier curves showing $Xrcc1^{Nes\text{-}cre}$ mice can survive up to 4 months of age. (**f**) Comparison of an adult $Xrcc1^{Nes\text{-}cre}$ animal with a wild type control, shows growth retardation and a smaller brain in the mutant animal. (**g**) Magnetic resonance imaging analysis of 3-month-old control and mutant brains show that the cerebellum is markedly affected by Xrcc1 loss (white boxes). 3D volumetric analysis indicates ~30% reduction in cerebellar size expressed as relative units.

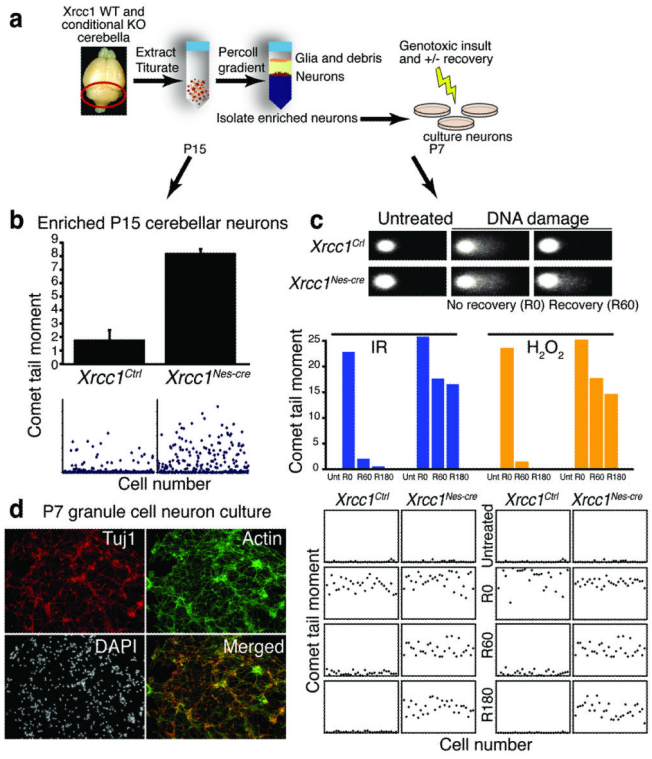

Figure 2. *Xrcc1*$^{Nes\text{-}cre}$ cerebellar granule neurons are DNA repair deficient

(**a**) A single-cell cerebella suspension was passed through a 35-60% percoll gradient and neurons at the interface were isolated for experiments. (**b**) Freshly isolated granule neurons were used to determine endogenous DNA strand breaks in the *Xrcc1*$^{Nes\text{-}cre}$ cerebellum (P15) via alkali comet analysis (ACA). Comet data from 250 individual neurons are plotted as the mean comet tail moment (bar graph) and individual comet tail moments from these neurons are shown (scatter plot). (**c**) *Xrcc1*$^{Nes\text{-}cre}$ cerebellar granule neurons (P7) are defective in DNA repair after ionizing radiation (20Gy) or 100μM H_2O_2. Various periods post-damage were examined (0 minute [R0], 60 minutes [R60], 180 minutes [R180]). Photomicrographs of representative damaged and repaired neurons following ACA are shown for both *Xrcc1*$^{Nes\text{-}cre}$ and control neurons. Mean comet tail moments for each time point are represented on a bar graph, while tail moment data for 30 representative neurons are shown on a scatter plot. (**d**) Cultured granule neurons are immunopositive for Tuj1 (β–tubulin III), a marker of postmitotic neurons (mag. ×40).

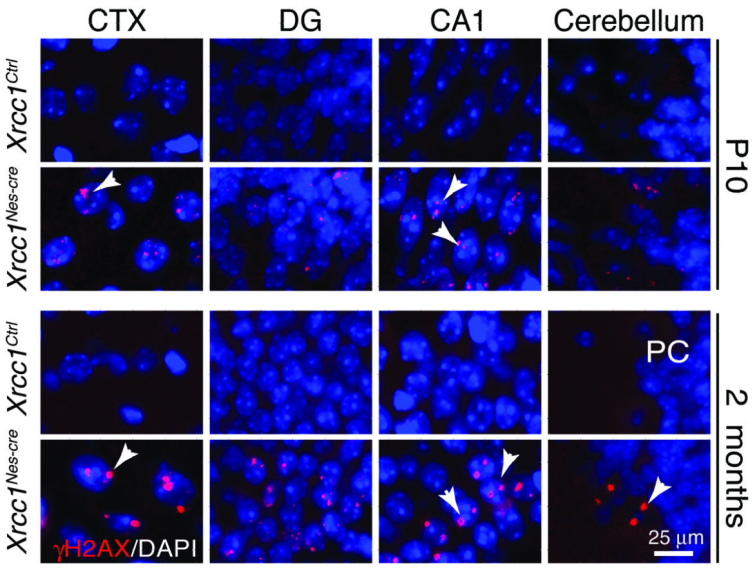

Figure 3. The *Xrcc1*-deficient brain accumulates DNA damage in mature neurons

DNA damage accumulates in different $Xrcc1^{Nes\text{-}cre}$ brain regions progressively with age as measured by γH2AX foci (arrows) at postnatal day 10 (P10) and 2 months of age. CTX; cerebral cortex, DG; the dentate gyrus of the hippocampus, CA1; the CA1 region of the hippocampus, PC; Purkinje cell layer.

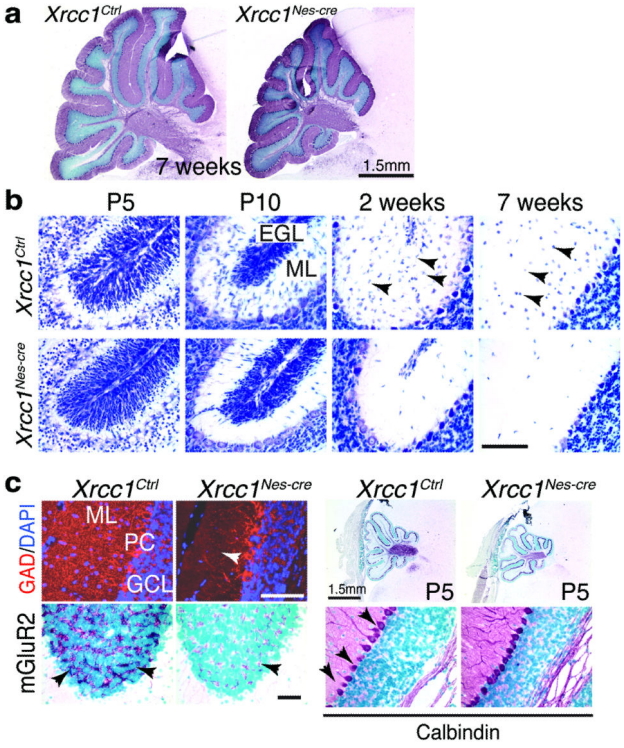

Figure 4. Interneurons are missing in the *Xrcc1*$^{Nes\text{-}cre}$ cerebellum

(**a**) Comparative view of 7-week-old wild type and *Xrcc1*$^{Nes\text{-}cre}$ cerebella after calbindin immunostaining; although smaller, histology of the mutant cerebellum is similar to wild type. (**b**) Nissl staining at different ages indicates the presence of interneurons in the molecular layer of the control cerebellum (arrows), but an absence from the *Xrcc1*$^{Nes\text{-}cre}$ cerebellum. EGL; external granule layer, ML; molecular layer, P; postnatal day. (**c**) Glutamic acid decarboxylase (GAD) immunostaining identifies GABAergic neurons (upper panels) which are absent in the *Xrcc1*$^{Nes\text{-}cre}$ tissue (white arrow). Metabotropic glutamate receptor 2 (mGluR2) staining (black arrows, lower panels) identifies Golgi cells in the granule layer. Calbindin staining of Purkinje cells identifies a similar organization of the Purkinje layer between the wild type and mutant cerebella (black arrows). GCL; granule cell layer, PC; Purkinje layer. Except where indicated, scale bars are 200μm.

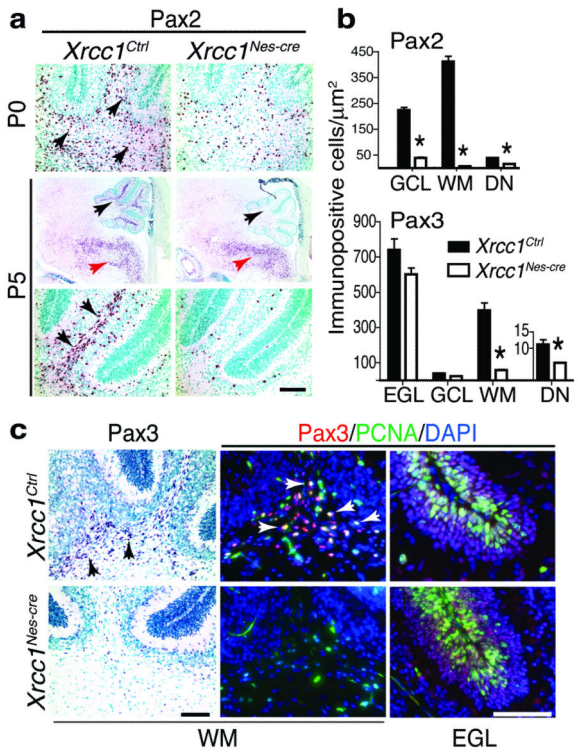

Figure 5. Differentiating interneurons decrease in the *Xrcc1*$^{Nes\text{-}cre}$ cerebellum

(**a**) Pax2 identifies differentiating interneurons in the white matter (WM) of the developing postnatal control cerebellum (black arrows). The *Xrcc1*$^{Nes\text{-}cre}$ cerebellum showed a substantial reduction of Pax2-positive cells from birth (P0) and by P5 interneurons were almost absent. In contrast, Pax2-positive cells in the brainstem remained unaffected (red arrows, middle panels). (**b**) Quantification of Pax immunostaining averaged from 3 different animals in the cerebellar EGL, GCL, WM and deep nucleus at P7. The asterisk indicates statistically significant (±s.e.m.) differences ($p<0.05$). (**c**) Pax3-positive cells in the WM are also reduced in the *Xrcc1*$^{Nes\text{-}cre}$ cerebellum from birth and are absent by P7. Many Pax3 (red) positive cells co-stain with PCNA (green) in the control P7 cerebellum but not in *Xrcc1*$^{Nes\text{-}cre}$ WM. However, the distribution of Pax3-positive cells is similar in both WT and *Xrcc1*$^{Nes\text{-}cre}$ EGL. The white arrows indicate cells that are immunopositive for both Pax3 and PCNA. EGL; external germinal layer, GCL; granule cell layer, WM; white matter, DN; deep nucleus, P; postnatal day. DAPI is 4,6-Diamidino-2-Phenylindole. Scale bar is 200μm.

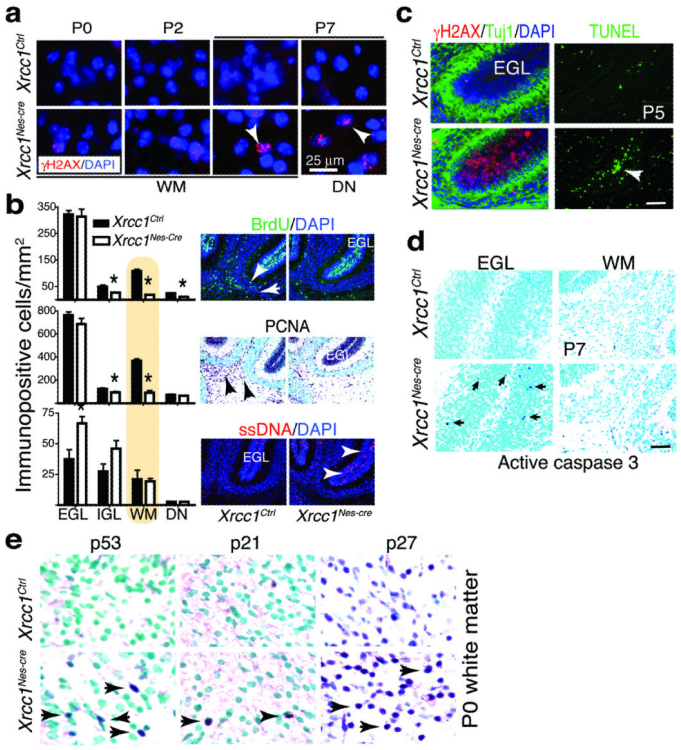

Figure 6. Cell cycle arrest in response to DNA damage in the *Xrcc1*$^{Nes\text{-}cre}$ cerebellum

(**a**) DNA damage accumulates in the *Xrcc1*$^{Nes\text{-}cre}$ white matter (WM) and deep nucleus (DN) (lower panels) but not in control tissue (upper panels) as shown by γH2AX formation. Nuclei are stained with DAPI. (**b**) Quantification of cells positive for cell cycle (BrdU and PCNA) or apoptosis (ssDNA) markers in the EGL, IGL, WM and DN of the developing cerebellum at P7. The asterisk indicates statistically significant (±s.e.m.) comparisons ($p<0.05$). Inset panels show immunohistochemistry for each genotype and the respective markers used for quantification. (**c**) Although γH2AX also forms in the EGL, in contrast to the WM, robust apoptosis occurs in the EGL as judged by TUNEL that coincides with γH2AX foci (lower panels). (**d**) Caspase-3 activation occurs in the P7 *Xrcc1*$^{Nes\text{-}cre}$ EGL but not in the *Xrcc1*$^{Nes\text{-}cre}$ WM. (**e**) p53, p21 and p27 markers of cell cycle arrest are found in the white matter of the *Xrcc1*$^{Nes\text{-}cre}$ cerebellum during postnatal development (arrows). EGL; external germinal layer, GCL; granule cell layer, WM; white matter and DN; deep nucleus. DAPI is 4,6-Diamidino-2-Phenylindole. Except where indicated, scale bars are 200μm.

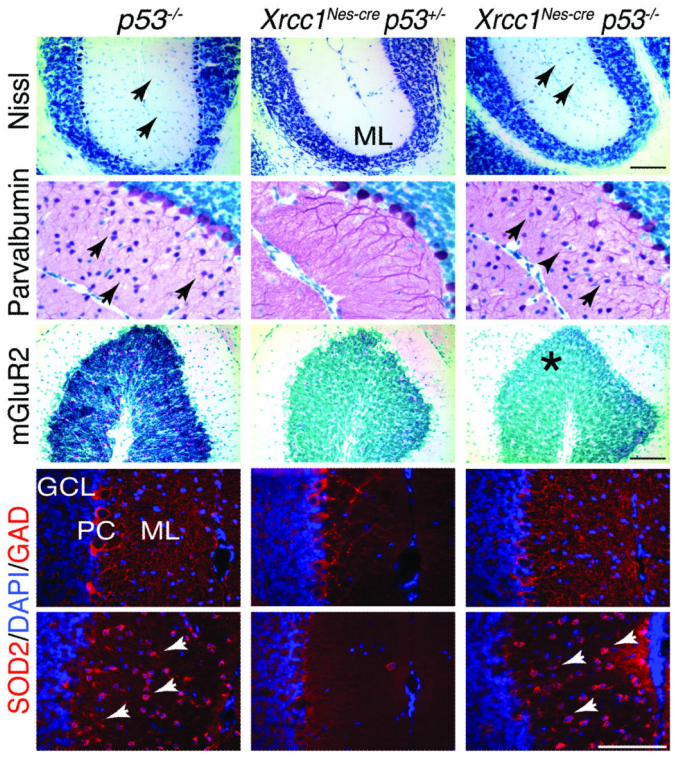

Figure 7. Interneuron loss in the *Xrcc1*-null cerebellum is dependent upon p53

Loss of p53 rescued stellate and basket interneurons in the *Xrcc1*$^{Nes\text{-}cre}$;*p53*$^{-/-}$ cerebellum as shown by Nissl and parvalbumin staining (arrows). In contrast, p53 loss was less effective at restoring Golgi interneurons in the granule cell layer (GCL) as determined by mGluR2 staining (asterisk). Glutamic acid decarboxylase (GAD) immunostaining showed restored synaptic density in the *Xrcc1*$^{Nes\text{-}cre}$;p53$^{-/-}$ molecular layer (ML), as did superoxide dismutase 2 (SOD2) immunostaining (arrows). PC is the Purkinje cell layer. DAPI is 4,6-Diamidino-2-Phenylindole. Scale bars are 200μm.

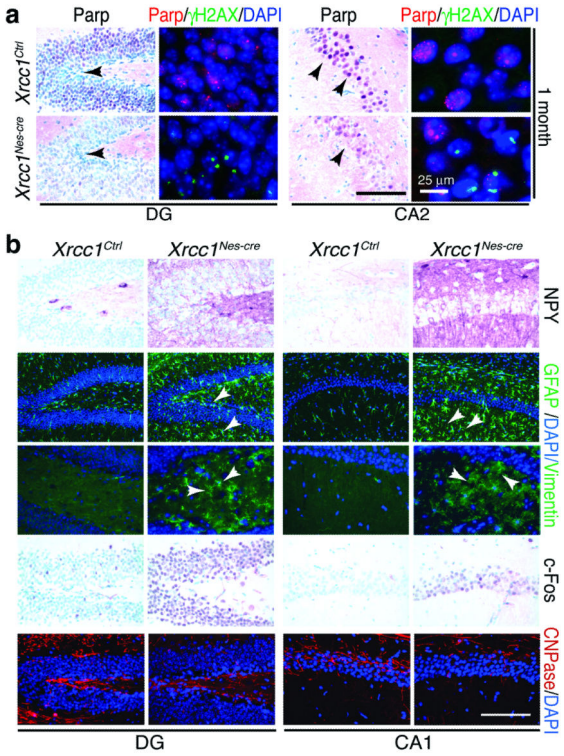

Figure 8. Loss of Xrcc1 affects hippocampal homeostasis

(**a**) Levels of the Xrcc1-binding protein Parp1 are reduced in the mature *Xrcc1*$^{Nes\text{-}cre}$ hippocampus (arrows) and many cells accumulate DNA strand breaks, in the dentate gyrus (DG) and other hippocampal regions such as the CA2 region indicated by γH2AX foci. (**b**) Neuropeptide Y (NPY) immunostaining is increased in the *Xrcc1*$^{Nes\text{-}cre}$ hippocampus. Astrogliosis in the adult *Xrcc1*$^{Nes\text{-}cre}$ hippocampus is shown by increased GFAP and vimentin immunoreactivity (arrows). Increased c-Fos immunoreactivity indicates altered gene expression in the hippocampus after Xrcc1 loss. Reduced 2,3-Cyclic Nucleotide 3-Phosphodiesterase (CNPase) immunostaining indicates that oligodendrocytes are also affected in the *Xrcc1*$^{Nes\text{-}cre}$ hippocampus. DG, the dentate gyrus of the hippocampus; CA1, CA2 the CA1 and CA2 region of the hippocampus. DAPI is 4,6-Diamidino-2-Phenylindole. Except where indicated, scale bars are 200μm.